UNIVERSIDAD COMPLUTENSE DE MADRID

FACULTAD DE CIENCIAS FÍSICAS

Máster en Física Teórica

TRABAJO FIN DE MÁSTER

Cuantización de solitones topológicos en teorías de branas

Quantization of Topological Solitons in Brane Theories

Sergio Sánchez Rentero

Director/es:

José Alberto Ruiz Cembranos

Alberto García Martín-Caro

Curso Académico 2025-26

UNIVERSIDAD
COMPLUTENSE
MADRID

Declaración responsable sobre autoría y uso ético de herramientras de Inteligencia Artificial (IA)

Yo, Sergio Sánchez Rentero,

con DNI: 76064994S,

declaro de manera responsable que el presente Trabajo Fin de Máster (TFM) titulado:

Cuantización de solitones topológicos en teorías de branas

es el resultado de mi trabajo intelectual personal y creativo, y ha sido elaborado de acuerdo con los principios éticos y las normas de integridad vigentes en la comunidad académica y, más específicamente, en la Universidad Complutense de Madrid.

Soy, pues, la persona autora del material aquí incluido y, cuando no ha sido así y he tomado el material de otra fuente, lo he citado o bien he declarado su procedencia de forma clara —incluidas, en su caso, herramientas de inteligencia artificial—. Las ideas y aportaciones principales incluidas en este trabajo, y que acreditan la adquisición de competencias, son mías y no proceden de otras fuentes o han sido reescritas usando material de otras fuentes.

Asimismo, aseguro que los datos y recursos utilizados son legítimos, verificables y han sido obtenidos de fuentes confiables y autorizadas. Además, he tomado medidas para garantizar la confidencialidad y privacidad de los datos utilizados, evitando cualquier tipo de sesgo o discriminación injusta en el tratamiento de la información.

En Madrid, a 8 de junio de 2026.

FIRMA

Quantization of Topological Solitons in Brane Theories

Sergio Sánchez Rentero

José Alberto Ruíz Cembranos
Departamento de Física Teórica, Universidad Complutense de Madrid

Alberto García Martín-Caro
Instituto de Física e Ciencias Aeroespaciais (IFCAE), Universidade de Vigo. 32004 Ourense, Spain

In this work, we investigate the canonical quantization of topological solitons in brane-world scenarios. We focus specifically on Brane-Skyrmions. These topological field configurations are similar to standard Skyrmions and emerge as solutions to the Dirac-Nambu-Goto action with an induced curvature term. By quantizing the spin collective coordinates of the Brane-Skyrmion, we find that the resulting Hamiltonian contains contributions at arbitrarily high orders in J^2. This provides a clear advantage over the standard Skyrme model. Furthermore, we implement a Physics-Informed Neural Network (PINN) to find the soliton profile that minimizes the energy, properly incorporating the backreaction from the quantized spin degrees of freedom. Finally, we discuss the potential applications of this framework to describe hadronic spectra. These results show the theoretical potential of brane-defect models and the increasing importance of neural networks in theoretical physics.

Declaration of AI Usage: It is hereby stated that Large Language Models (LLMs) have been used solely to assist with the grammatical review and linguistic optimization of the English text. These tools were employed in a strictly secondary capacity and played no role in generating original ideas or theoretical developments presented in this work.

I. INTRODUCTION

The concept of extra spatial dimensions dates back to the pioneering works of Kaluza and Klein [1, 2], who attempted to unify electromagnetism and gravity. In modern theoretical physics, this idea has evolved into the well-known "brane-world" scenario. In this framework, our observable universe is modeled as a four-dimensional hypersurface, the "brane", embedded within a higher-dimensional bulk space [3, 4].

The presence of a rigid brane in the bulk spontaneously breaks the translational invariance of the extra dimensions. According to Goldstone's theorem, this symmetry breaking gives rise to massless scalar fields on the brane, called "branons" [5]. Physically, these branons represent the transverse fluctuations of the brane into the extra dimensions. However, the mathematical structure of the vacuum manifold where these fields reside allows for more than simple perturbative oscillations. It can also support stable configurations known as topological defects. Intuitively, these defects occur when the field configuration "wraps" around the internal target space (co-dimensions) in a way that cannot be continuously deformed back to the trivial vacuum.

In this work, we are particularly interested in a specific type of topological soliton related to the Skyrme model [6, 7]. Originally formulated in the context of nuclear physics, the Skyrme model successfully describes baryons (such as protons and neutrons) as topological solitons emerging from the low-energy dynamics of pion fields, where the baryon number is identified with the topological charge of the soliton. Inspired by this success, we consider the framework developed in [5]. This framework demonstrates that the low-energy effective action for branons, derived from a Dirac-Nambu-Goto action with induced curvature terms, is topologically very similar to the chiral Lagrangians of QCD. As a consequence, this brane action also supports Skyrmion-like solutions, called "Brane-Skyrmions" [8].

However, Brane-Skyrmions arise in the context of a brane theory, while the Skyrme model arises from nuclear physics. The effective actions of both models are completely different. From this point of view, our motivation in this work is to investigate whether we can also describe baryons as Brane-Skyrmions and how their predictions differ from the Skyrme model. For that purpose, one must perform the quantization of these solitons, as there has only been an approximate classical description of solutions in the brane model [8]. Historically, this was achieved for the original Skyrme model by introducing time-dependent collective coordinates [9], allowing the soliton to rotate as a rigid body and therefore acquire quantized spin and isospin states.

We start by describing the Brane-Skyrmion model [8] at the classical level. In Section II, we introduce the standard notation and the underlying mathematical framework. This includes the symmetries of the model and relevant results, like the induced metric for the brane and the mass functional. Furthermore, we implement Physics-Informed Neural Networks (PINNs) as the computational tool to solve the highly non-linear differential equations governing the soliton profile. We also discuss the physical implications of the classical Brane-Skyrmions through Derrick's scaling argument [10]. After that, we proceed with the canonical quantization in

Section III by introducing a rigid rotation ansatz for the soliton into the highly non-linear effective action of the brane. This allows us to construct the quantum Hamiltonian for Brane-Skyrmions and develop a systematic perturbative approach in a slow-rotation regime, showing how the quantum centrifugal barrier stabilizes the soliton against collapse to a point-like defect. Finally, we perform a phenomenological fit of the quantized model to the empirical hadronic spectra.

II. CLASSICAL CONFIGURATIONS OF STATIC BRANE-SKYRMIONS

Effective action and mass. To keep the mathematical framework clear, we introduce the following standard notation for the coordinates of the manifolds under consideration:

- D-dimensional bulk spacetime: $\{X^A\}$, with $A = 0, \ldots, D-1$.
- d-dimensional world-volume: $\{x^\mu\}$, with $\mu = 0, \ldots, d-1$. The component x^0 is typically identified as the coordinate time.
- $\bar{d}$-dimensional (with $\bar{d} = D-d$) target space: $\{X^I\}$, with $I = d, \ldots, D-1$.

The effective action for the brane must inherit the bulk spacetime isometries through a set of global symmetries. Some of these might be nonlinearly realized (see e.g. [11]).

In addition, gauge symmetry requires the effective action to be invariant under reparameterization of the world-volume coordinates by arbitrary functions $\xi^\mu(x)$:

$$\delta_g X^A = \xi^\mu(x)\partial_\mu X^A. \tag{1}$$

We can use this gauge freedom to select the so-called unitary gauge for parameterizing the brane's world-volume [8]:

$$X^\mu(x) = x^\mu, \quad X^I(x) = \pi^I(x); \quad X^A(x) = (x^\mu, \pi^I(x)). \tag{2}$$

Here, π^I denotes the $\bar{d}$ fields representing the position of the brane along the extra dimensions. Physically, this means that an observer on the brane perceives the transverse fluctuations of the brane within the bulk space as a set of scalar fields. These correspond to Nambu-Goldstone modes (branons [8]) associated with the spontaneous symmetry breaking of the original isometry group.

Under these assumptions, the effective action for the brane, up to second order in derivatives, is given by [8]:

$$S = \int_{M_4} \mathrm{d}^4x\, \sqrt{g}(-f^4 + \lambda f^2 \mathcal{R} + \cdots), \tag{3}$$

where $\mathrm{d}^4x\,\sqrt{g}$ is the invariant volume element of the brane, $\mathcal{R}$ is the induced scalar curvature, λ is a coupling parameter, and f represents the brane tension.

To construct a topological soliton within our physical 3-dimensional space, the target space of the scalar fields must be 3-dimensional. We consider a four-dimensional space-time M_4 ($d = 4$) embedded within a bulk space containing exactly $\bar{d} = 3$ extra dimensions. We choose these extra dimensions to be S^3, which gives a $D = 7$ bulk [8]. Therefore, we model the bulk space as $M_4 \times S^3$, and the π^I fields representing the Brane-Skyrmions are mappings of the form $\pi^I : \mathbb{R}^3 \to K$ [8], where K is the coset space.

In this scenario, the original isometry group is $\mathrm{ISO}(1,3) \times \mathrm{SO}(4)$. The presence of the brane on the compact dimensions breaks this isometry down to $\mathrm{ISO}(1,3) \times \mathrm{SO}(3)$, yielding the coset space

$$K = \frac{\mathrm{ISO}(1,3) \times \mathrm{SO}(4)}{\mathrm{ISO}(1,3) \times \mathrm{SO}(3)} \cong \frac{\mathrm{SO}(4)}{\mathrm{SO}(3)} \cong S^3. \tag{4}$$

Assuming the branon fields π^I vanish at spatial infinity ($\pi^I \to 0$ as $r \to \infty$), the physical space $\mathbb{R}^3$ is effectively one-point compactified into S^3. The fields then constitute mappings $\pi^I : S^3 \to S^3$. This allows us to classify them according to the third homotopy group of K, which is $\pi_3(K) = \pi_3(S^3) = \mathbb{Z}$. Each mapping is characterized by an integer known as the winding number. This number serves as a topological invariant. Intuitively, it counts how many times the physical space "wraps" around the internal target space. The topological nature of the π^I fields ensures that Brane-Skyrmions represent stable, finite-energy configurations that cannot be continuously deformed into the trivial vacuum state ($\pi^I = 0$).

For static configurations, the Brane-Skyrmion mass is defined as [8]:

$$M_S[\pi] = \int_{M_3} \mathrm{d}^3x\, \sqrt{g}(-f^4 + \lambda f^2 \mathcal{R}) - M_S[0]. \tag{5}$$

This represents the energy strictly arising from the topological defect (the Brane-Skyrmion) on the brane. It explicitly ignores the infinite energy contribution from the flat background.

Hedgehog ansatz. To set up the mathematical framework clearly, we introduce spherical coordinates for the manifolds involved. In M_4, we denote the coordinates as $\{t, r, \theta, \phi\}$, with $\phi \in [0, 2\pi)$, $\theta \in [0, \pi)$, and $r \in [0, \infty)$. In the coset manifold $K \sim S^3$, the Cartesian coordinates are the branon fields, denoted by $\{\pi^I\}$. We denote the spherical coordinates of S^3 as $\{\chi_K, \theta_K, \phi_K\}$, with $\phi_K \in [0, 2\pi)$ and $\theta_K, \chi_K \in [0, \pi)$.

Throughout this work, we assume the *hedgehog ansatz*. This highly symmetric configuration correlates the spatial directions with the internal field directions. It causes the field to point radially outward from the center, much like the spines of a hedgehog. Mathematically, the Brane-Skyrmion with winding number n_W is given by the nontrivial mapping $\pi^I : S^3 \to S^3$, defined by $\phi_K = \phi$, $\theta_K = \theta$, and $\chi_K = F(r)$. It is subject to the boundary

conditions $F(0) = n_W\pi$ and $F(\infty) = 0$. As a result, the spherical coordinates in S^3 relate to the physical branon fields via [8]:

$$\begin{aligned}\pi^1(x) &= v\sin F(r)\sin\theta\cos\phi,\\ \pi^2(x) &= v\sin F(r)\sin\theta\sin\phi,\\ \pi^3(x) &= v\sin F(r)\cos\theta,\end{aligned} \tag{6}$$

where v represents the radius of the 3-sphere.

With these coordinates, the induced metric on the brane (M_4) takes a simple diagonal form [8]:

$$g_{\mu\nu} = \mathrm{diag}\left(1, -B(r), -\rho^2(r), -\rho^2(r)\sin^2\theta\right), \tag{7}$$

where

$$B(r) = 1 + \frac{v^2}{f^4}F'^2(r), \quad \rho^2(r) = r^2 + \frac{v^2}{f^4}\sin^2 F(r). \tag{8}$$

We derive this metric directly from the geometry of the bulk space using the following expression [8]:

$$g_{\mu\nu} = \tilde{g}_{\mu\nu} - \frac{1}{f^4}h_{IJ}(\pi)\partial_\mu\pi^I\partial_\nu\pi^J, \tag{9}$$

where $\tilde{g}_{\mu\nu}$ is the background metric on the brane. In our setup, this is the Minkowski metric $\eta_{\mu\nu}$ with signature $(+,-,-,-)$. The tensor $h_{IJ}(\pi)$ represents the metric of the coset space K, which is a 3-sphere with signature $(+,+,+)$.

Finally, we can express the Brane-Skyrmion mass (5) as a functional of $F(r)$ by computing the determinant $\sqrt{g}$ and the scalar curvature $\mathcal{R}$ from the metric [8]:

$$\sqrt{g} = \sqrt{B(r)}\rho^2(r)\sin\theta, \quad \mathcal{R} = -\frac{2}{\rho^2}\left(1 - \frac{1}{A}\right) - \frac{2A'}{A^2\rho\rho'}, \tag{10}$$

where $A(r) = B(r)/\rho'^2(r)$.

Atiyah-Manton ansatz. Now that we can express the Brane-Skyrmion mass as a functional $M_S[F]$, we can minimize it using standard methods. This allows us to obtain both the soliton profile $F(r)$ and the total energy of the configuration. Before moving to the general case[1], we recall the Atiyah-Manton ansatz [12] for a $n_W = 1$ soliton:

$$F(r) = \pi\left(1 - \frac{1}{\sqrt{1 + (L/r)^2}}\right), \tag{11}$$

where L is a parameter characterizing the size of the soliton.

This ansatz was originally derived from the holonomy of Yang-Mills instantons in $\mathbb{R}^4$ [12]. It accurately reproduces the solution of the original $SU(2)$ Skyrme model in QCD chiral dynamics [6, 7, 9]. Because of this success, the authors in [8] used it to approximate the Brane-Skyrmion profile, given its close resemblance to standard Skyrmions.

By adopting the Atiyah-Manton ansatz (11), the mass functional reduces to an ordinary function of L. We can then find the energy of the configuration simply by minimizing $M_S(L)$ with respect to this parameter. The optimal value, denoted as L_m, depends directly on λ (see Figure 4 in [8]):

$$\left.\frac{\mathrm{d}M_S}{\mathrm{d}L}\right|_{L_m} = 0 \;\rightarrow\; M_S \equiv M_S(L_m),\; L_m = L_m(\lambda). \tag{12}$$

While this ansatz has been studied for Brane-Skyrmions in [8], it remains unclear whether it provides a sufficiently accurate approximation to the true minimum of the energy functional.

Numerical solution. As noted in [8], minimizing the general case without assuming the Atiyah-Manton ansatz for the profile function (11) requires solving a complex second-order differential equation. While standard numerical methods can solve it with enough computational effort, we introduce a more powerful approach that will be highly advantageous when addressing the quantum case: Physics-Informed Neural Networks (PINNs).

Standard machine learning models require large datasets to learn interpolations. We provide further details on this in Appendix B, which the reader can skip without losing continuity. In contrast, PINNs act as unsupervised differential equation solvers. By evaluating the gradients of the neural network with respect to the input coordinates via automatic differentiation, the network optimizes its weights to minimize the energy functional directly.

To implement a PINN for our minimization problem, we first define the architecture of the network using the following expression for the soliton profile, $F(r)$:

$$F(r) = F_0(r) + V(r)N(r), \tag{13}$$

where:

- $F_0(r)$ is an initial ansatz for the solution that satisfies the boundary conditions $F_0(0) = \pi$ and $F_0(\infty) = 0$. The Atiyah-Manton ansatz (11), for instance, can serve this purpose.
- $N(r)$ is the output of the neural network, parameterized by its weights and biases. This function modifies the initial ansatz $F_0(r)$ to reach the true solution $F(r)$ that minimizes the energy functional.
- $V(r)$ is a weight function for the variation of $F_0(r)$, satisfying the boundary conditions $V(0) = V(\infty) = 0$. The following choice yields reasonable results for our purposes:

$$V(r) = \frac{L_m}{L_m + r}e^{-\epsilon^2/r^2}e^{-\epsilon^2/(r-r_{\max})^2}, \tag{14}$$

[1] Throughout this work, we use "the general case" to refer to $F(r)$ without specifying a radial ansatz, though we maintain the hedgehog configuration and all previous assumptions.

where $r_{\max}$ is the numerical integration cutoff, and ϵ is a length scale that controls the steepness of the function. In this work, we use $\epsilon = 10^{-5}$ because it best reproduces the results from traditional numerical methods. The parameter L_{m} is the optimal length scale found by minimizing the energy with the Atiyah-Manton ansatz, determining the characteristic size of the soliton.

With the architecture established, we can outline the workflow of our model, which closely resembles a gradient flow method. The input for the neural network is a set of values for the radial coordinate r. We feed the network a column vector containing N_r points distributed between 0 and the maximum radial distance $r_{\max}$ that we want to evaluate, as integrating to infinity is computationally prohibitive. We define two hidden layers with 40 neurons each. A Gaussian Error Linear Unit (GELU) activation function is applied to each layer to provide a smooth nonlinear transformation[2]. Every hidden layer contains weights and biases, representing the network parameters θ_i, which are updated after every iteration.

The network outputs the function $N(r)$ introduced in (13). We then evaluate the mass functional (5) using the full profile $F(r)$ constructed from this output to compute the energy of the configuration. During each iteration, the model calculates the gradient of this energy with respect to each network parameter θ_i, denoted as $\partial M_S/\partial\theta_i$. The optimizer then determines the direction to update these parameters in the next step to minimize M_S. We find that the Adam optimizer is sufficient for our purposes.

We implemented this PINN using the PyTorch library in Python, and the code is publicly available at [14]. Our script is loosely based on lecture notes regarding PINNs for strong gravity and PDE solving by Raimon Luna [15].

Let us now examine the numerical results produced by the PINN. Since this method does not mathematically guarantee convergence to a global minimum of the energy, to verify the reliability of our results we provide, without loss of continuity a validation for the static case in Appendix A. Figures 1 and 2 show the solutions for two different values of the rescaled parameter $\lambda^* = \lambda/f^2R_B^2$. We also compare the profiles obtained by the PINN against those calculated using a traditional shooting method.

As we will discuss later, the solution becomes point-like as $\lambda \to 0$. However, it remains topologically non-trivial because its mass satisfies a strict topological bound [8]. For values around $\lambda^* \sim 1$, the Atiyah-Manton ansatz (11) provides a solid approximation to the exact solution for static Brane-Skyrmions (see Figure 1) [8]. However, our

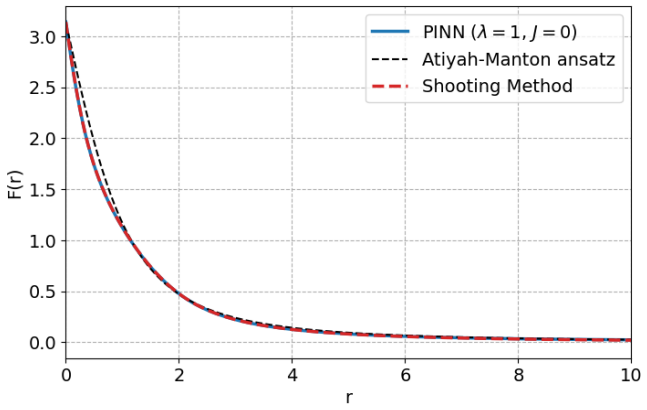

FIG. 1. Neural network solution for a static ($J = 0$) Brane-Skyrmion with $\lambda^* = 1$, compared to the Atiyah-Manton and Shooting method solutions.

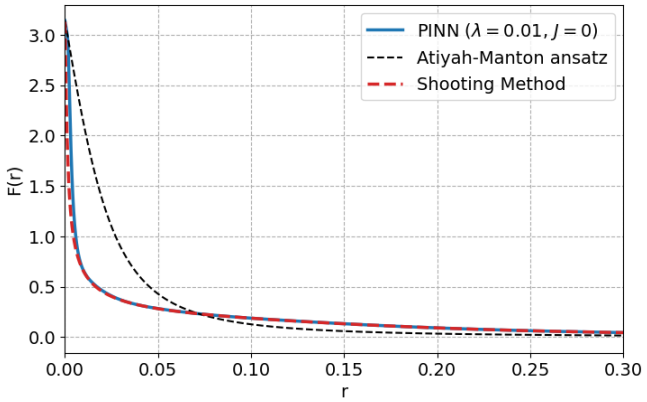

FIG. 2. Neural network solution for a static ($J = 0$) Brane-Skyrmion with $\lambda^* = 0.01$, compared to the Atiyah-Manton and Shooting method solutions.

results show a clear deviation for small values of λ (see Figure 2) as the soliton becomes progressively point-like.

We can understand this discrepancy through Derrick's theorem [10] (for a detailed discussion, see [16], Sec. 4.2). This theorem analyzes how the total energy $E(L)$ of a soliton changes when we rescale its profile as $F(r) \to F(r/L)$. In the Skyrme model, the total energy scales as follows [16]:

$$E_{\mathrm{Skyrmion}}(L) = E_2 L + \frac{E_4}{L}, \tag{15}$$

where E_2 and E_4 are constants.

As $L \to 0$, the E_4 term diverges, which physically prevents a stable Skyrmion from collapsing to a point. On the other hand, the energy also diverges as $L \to \infty$. Therefore, a stable configuration must have a non-zero, finite size. This is a highly desirable feature for describing nucleons. The Atiyah-Manton ansatz (11) is specifically designed to capture exactly this type of configuration.

On the other hand, Derrick's theorem yields entirely

[2] The smoothness and differentiability of the activation function are crucial to ensure that derivatives obtained via automatic differentiation remain well defined and numerically stable. See [13] for a systematic analysis of activation function choices in PINNs.

different implications for Brane-Skyrmions. Let us evaluate the mass functional (5) in the limit $\lambda \to 0$ (neglecting the contribution from the induced curvature of the brane) and apply the Derrick scaling $r = L\tilde{r}$:

$$E_{\rm BS}(L) \propto f^4 \int \mathrm{d}\tilde{r}\, L \left[\sqrt{1+\frac{R_B^2}{L^2}F'^2}(L^2\tilde{r}^2 + R_B^2 \sin^2 F)\right], \tag{16}$$

where $R_B = v/f^2$ represents the characteristic size of the soliton, and the derivative $F' \equiv \mathrm{d}F/\mathrm{d}\tilde{r}$ introduces the extra $1/L$ factor.

In the strict $L \to 0$ limit, the square root can be approximated as $\frac{R_B}{L}F'$. This cancels the overall L factor outside the bracket and results in a finite energy:

$$\lim_{L\to 0} E_{\rm BS}(L) \propto \int_0^\infty \mathrm{d}\tilde{r}\, f^4 R_B^3 F' \sin^2 F > 0. \tag{17}$$

As a result, a Brane-Skyrmion can become point-like while maintaining a completely finite energy. The Atiyah-Manton ansatz simply cannot handle this scenario, as point-like solitons with finite energy only appear in brane theories. This analysis also provides the correct normalization for the mass [8]:

$$M_S(\lambda \to 0) = 4\pi f^4 R_B^3 \int_0^\pi \mathrm{d}u \sin^2 u = 2\pi^2 f^4 R_B^3, \tag{18}$$

where the factor of 4π comes from the angular integration. We introduce the change of variable $u = F(\tilde{r})$ to solve the radial integral analytically, only with the boundary conditions, without knowing the explicit form of $F(\tilde{r})$.

III. QUANTIZATION OF SPHERICAL BRANE-SKYRMIONS

Up to this point, we have reviewed several known properties of Brane-Skyrmions previously discussed in [8], while also analyzing new physical implications. However, these are strictly static configurations that lack any notion of angular momentum. In addition, we have demonstrated that these static solitons can admit point-like configurations. These characteristics fail to accurately describe physical particles. For this reason, the quantization of Brane-Skyrmions becomes necessary.

To simplify the complex calculations, we will maintain the hedgehog ansatz (6). This restricts our quantization to spherical configurations of Brane-Skyrmions, meaning those fully described by the one-dimensional profile $F(r)$.

This raises a fundamental question: which degrees of freedom should we quantize, and how can we introduce the notion of angular momentum to static Brane-Skyrmions? To address these questions, we take inspiration from the canonical quantization of classical Skyrmions [9]. We first recall the expression for the induced metric on the brane:

$$g_{\mu\nu} = \eta_{\mu\nu} - \frac{1}{f^4} h_{IJ}(\pi)\partial_\mu \pi^I \partial_\nu \pi^J. \tag{19}$$

Since this metric is quadratic in the π^I fields, it is manifestly invariant under global $SO(3)$ rotations, $\pi^I = R^I_J \pi^J$, where $R \in SO(3)$ is independent of the space-time coordinates. As a result, the effective action for Brane-Skyrmions is globally $SO(3)$-invariant, meaning that rotating a static solution requires no potential energy cost. These continuous symmetries correspond to zero-modes of the classical system. We can promote them to dynamical collective coordinates by making the transformation parameters time-dependent:

$$\pi^I(t) = R^I_J(t)\pi^J_0, \quad R(t) := e^{t\omega_i L^i}, \tag{20}$$

where π^I_0 denotes the static branon fields[3] (6), $L^i \in \mathfrak{so}(3)$ are the generators of the $SO(3)$ group, and ω_i are three real parameters.

The expression chosen for $R(t)$ can be interpreted physically as a rigid-body rotation ansatz. Here, ω_i represents the components of the angular velocity along the three spatial axes. Later, we will assume a slow-rotation regime to properly justify this rigid ansatz.

Effective Lagrangian. We begin by computing the new effective Lagrangian under the rotation ansatz (20). We could do this using a general time-dependent rotation, but we maintain the rigid rotation ansatz for simplicity. Because the action lacks second-order time derivatives, we could safely substitute $\omega^i \equiv \dot{\theta}^i(t)$ at each step of the derivation, where $\theta^i(t) = t\omega^i$ describes the rigid rotation.

The first step is to calculate the induced metric on the brane. We write it as:

$$g_{\mu\nu} = \eta_{\mu\nu} - G_{\mu\nu}(\pi), \quad G_{\mu\nu}(\pi) = \frac{1}{f^4} h_{IJ}(\pi)\partial_\mu \pi^I \partial_\nu \pi^J, \tag{21}$$

where $\pi^I \equiv \pi^I(t)$ now represents the dynamical field configurations.

Next, we explicitly compute the metric $h_{IJ}(\pi)$ using the Cartesian coordinates $\{\pi^I\}$ of the coset space. Since the coset space is isomorphic to S^3, we embed it into $\mathbb{R}^4$ with the coordinates (Y^0, π^I) subject to the following constraint:

$$(Y^0)^2 + \pi^2 = v^2 \quad \Rightarrow \quad \mathrm{d}Y^0 = -\frac{\pi_I\, \mathrm{d}\pi^I}{\sqrt{v^2 - \pi^2}}, \tag{22}$$

where v is the radius of the 3-sphere, and $\pi^2 \equiv \pi_I \pi^I$. Note that indices are risen and lowered with δ_{IJ}: $\pi_I = \delta_{IJ}\pi^J$.

This gives the following line element for the coset space:

$$\mathrm{d}{S_K}^2 = \delta_{IJ}\, \mathrm{d}\pi^I\, \mathrm{d}\pi^J + \frac{\pi_I\, \mathrm{d}\pi^I\, \pi_J\, \mathrm{d}\pi^J}{v^2 - \pi^2}, \tag{23}$$

[3] Note that both $\pi^I(t)$ and π^I_0 also depend on the spatial coordinates $\{r, \theta, \phi\}$. We will omit this explicit dependence for the rest of this work for simplicity.

which leads directly to the metric tensor:

$$h_{IJ}(\pi) = \delta_{IJ} + \frac{\pi_I \pi_J}{v^2 - \pi^2}. \tag{24}$$

We now evaluate the components of $G_{\mu\nu}(\pi)$ defined in (21). The purely spatial components $G_{ij}(\pi)$ remain invariant under time-dependent rotations, as the time dependence only affects terms that involve temporal derivatives.

As a result, the spatial metric in the coordinate system $\{r, \theta, \phi\}$ takes the same form as in the static case (7):

$$g_{ij} = \text{diag}\left(-B(r), -\rho^2(r), -\rho^2(r)\sin^2\theta\right). \tag{25}$$

To evaluate the $G_{00}(\pi)$ component, we first need to compute $\partial_t R$. Using (20), we get:

$$\partial_t R^I_J = \omega^i (L_i)^I_K R^K_J = \epsilon^I{}_{iK} \omega^i R^K_J, \tag{26}$$

where we adopt the following representation for the generators:

$$(L_i)^I_J = \epsilon^I{}_{iJ}, \quad [L_i, L_j] = \epsilon_{ijk} L^k. \tag{27}$$

Note that the indices $I, J, K, \ldots$ correspond to the internal coset space, while $i, j, k, \ldots$ refers to the spatial manifold M_3 (which is $\mathbb{R}^3$). We then obtain the following expressions:

$$\dot{\pi}^I = \partial_t R^I_J \pi^J_0 = \epsilon^I{}_{iJ} \omega^i \pi^J, \tag{28}$$

$$\pi_I \dot{\pi}^I = \epsilon^I{}_{iJ} \pi_I \omega^i \pi^J = 0, \tag{29}$$

$$\dot{\pi}_I \dot{\pi}^I = \epsilon_{IiJ} \epsilon^I{}_{jK} \omega^i \pi^J \omega^j \pi^K = \omega^2 \pi^2 - (\omega^i \pi_i)^2, \tag{30}$$

where we applied the total antisymmetry of the Levi-Civita tensor ϵ_{ijk} alongside this identity: $\epsilon_{IiJ}\epsilon^I{}_{jK} = \delta_{ij}\delta_{JK} - \delta_{iK}\delta_{Jj}$. With that, we have:

$$G_{00}(\pi) = \frac{1}{f^4} h_{IJ}(\pi) \dot{\pi}^I \dot{\pi}^J = \frac{1}{f^4} \dot{\pi}_I \dot{\pi}^I \equiv \frac{\dot{\pi}^2}{f^4}. \tag{31}$$

and thus: $g_{00} = 1 - \frac{\dot{\pi}^2}{f^4}$.

We compute the mixed components $G_{0i}(\pi)$ in a similar manner, obtaining:

$$G_{0i}(\pi) = \frac{1}{f^4} h_{IJ}(\pi) \dot{\pi}^I \partial_i \pi^J = \frac{1}{f^4} \dot{\pi}_I \partial_i \pi^I. \tag{32}$$

and thus: $g_{0i} = -\frac{1}{f^4} \dot{\pi}_I \partial_i \pi^I$.

Gathering these results, the induced metric on the brane takes the following form:

$$g_{\mu\nu} = \begin{pmatrix} 1 - \frac{\dot{\pi}^2}{f^4} & -\frac{1}{f^4} \dot{\pi}_I \partial_i \pi^I \\ -\frac{1}{f^4} \dot{\pi}_I \partial_i \pi^I & g_{ij}(\pi_0) \end{pmatrix}. \tag{33}$$

We note that (33) remains valid regardless of the field ansatz. We now impose both assumptions, (6) and (20), to derive a more explicit version of the metric. Without loss of generality, we align the rotation axis with the z-axis. Because the hedgehog ansatz is spherically symmetric, the resulting inertia tensor is purely isotropic ($I_{ij} = \mathcal{I}\delta_{ij}$). Any arbitrary choice for the rotation axis yields an identical integrated Lagrangian. We set:

$$\boldsymbol{\omega} = (0, 0, \omega), \quad R(t) = \begin{pmatrix} \cos(\omega t) & -\sin(\omega t) & 0 \\ \sin(\omega t) & \cos(\omega t) & 0 \\ 0 & 0 & 1 \end{pmatrix}. \tag{34}$$

Taking these conditions into account, we find:

$$\dot{\pi}^2 = \omega^2 \pi^2 - (\omega^i \pi_i)^2 = v^2 \omega^2 \sin^2 F \sin^2\theta, \tag{35}$$

$$\dot{\pi}_I \partial_i \pi^I = \epsilon_{IjJ} \omega^j \pi^J \partial_i \pi^I = v^2 \sin^2 F \omega \sin^2\theta \delta^\phi_i, \tag{36}$$

where we use the relations $\pi_3 = \pi_{0,3}$ and

$$\pi_1 \partial_i \pi_2 - \pi_2 \partial_i \pi_1 = \pi_{0,1} \partial_i \pi_{0,2} - \pi_{0,2} \partial_i \pi_{0,1} \tag{37}$$

Note that the hedgehog ansatz (6) applies exclusively to the static fields π_0.

This yields the explicit induced metric:

$$g_{\mu\nu} = \begin{pmatrix} 1 - \omega^2 \Lambda(r) \sin^2\theta & 0 & 0 & -\omega\Lambda(r)\sin^2\theta \\ 0 & -B(r) & 0 & 0 \\ 0 & 0 & -\rho^2 & 0 \\ -\omega\Lambda(r)\sin^2\theta & 0 & 0 & -\rho^2 \sin^2\theta \end{pmatrix}, \tag{38}$$

where

$$\Lambda(r) = \rho^2(r) - r^2 = \frac{v^2}{f^4} \sin^2 F(r). \tag{39}$$

The non-vanishing $g_{0\phi}$ component reflects a frame-dragging effect in the azimuthal direction. This implies the soliton experiences a dynamical coupling along the rotational plane.

Our goal now is to compute the invariant volume element $\sqrt{g}$ and the scalar curvature $\mathcal{R}$. The metric determinant is straightforward to calculate:

$$g = g_0 \left(1 - \frac{r^2 \Lambda(r)}{r^2 + \Lambda(r)} \omega^2 \sin^2\theta\right), \tag{40}$$

where $g_0 = g_{rr} g_{\theta\theta} g_{\phi\phi}$ represents the determinant of the static Brane-Skyrmion metric.

We can then write:

$$\sqrt{g} = \sqrt{B(r)} \rho^2(r) \sin\theta \sqrt{1 - C(r)\omega^2 \sin^2\theta}, \tag{41}$$

where $B(r)$ and $\rho^2(r)$ are given by (8), and

$$C(r) = \frac{r^2 \Lambda(r)}{r^2 + \Lambda(r)} = \frac{v^2}{f^4} \frac{r^2 \sin^2 F(r)}{r^2 + \frac{v^2}{f^4} \sin^2 F(r)}. \tag{42}$$

Thus, $\sqrt{g}$ depends explicitly on ω^2. This result is perfectly consistent with the spherical symmetry imposed by the hedgehog ansatz.

Computing the scalar curvature $\mathcal{R}$ analytically by hand is prohibitively complex. We solve this by using symbolic computation in Wolfram Mathematica. The

resulting expression is extremely lengthy, so we omit it here. The interested reader can find the full notebook with the result at [14].

Finally, the effective Lagrangian density for dynamical Brane-Skyrmions retains the formal structure of the static case:

$$\mathcal{L}_{\text{eff}} = (-f^4 + \lambda f^2 \mathcal{R})\sqrt{g}, \tag{43}$$

where $\sqrt{g}$ is now given by (41) and $\mathcal{R}$ comes from our Mathematica evaluation.

Canonical quantization. In the previous section, we derived the effective Lagrangian in terms of ω^2. This represents the dynamical degree of freedom we want to quantize using the collective coordinates formalism [9].

The canonical momentum conjugate to ω corresponds to the angular momentum of the Brane-Skyrmion:

$$J = \frac{\partial L(\omega)}{\partial \omega}, \tag{44}$$

where $L(\omega)$ is the total effective Lagrangian:

$$L(\omega) = \int \mathrm{d}^3x \, \sqrt{g}(-f^4 + \lambda f^2 \mathcal{R}). \tag{45}$$

Note that we must use the total integrated Lagrangian, rather than just the Lagrangian density. Using the density would yield an incorrect canonical conjugate for ω, leading to a wrong Hamiltonian. Since the Hamiltonian is the main focus of our quantization scheme, this distinction is crucial.

If we could invert the relation $J = J(\omega)$ to obtain $\omega = \omega(J)$, we could easily construct the Hamiltonian of the system in terms of the canonical momentum J:

$$H(J) = J\omega(J) - L[\omega(J)]. \tag{46}$$

However, recall that $L(\omega)$ depends on ω^2 through a square root inside an integrand evaluated over all space. This makes it analytically impossible to invert the relation $J = J(\omega)$ exactly. To bypass this, we rely on the rigid rotation regime (20) assumed earlier, which requires ω to be a small quantity. As a result, we can expand $L(\omega)$ around $\omega = 0$ in powers of ω^2:

$$L(\omega) = -\alpha + \beta\omega^2 + \gamma\omega^4 + \mathcal{O}(\omega^6), \tag{47}$$

where α, β, γ, and all higher-order coefficients represent distinct positive-definite spatial integrals involving terms from $\sqrt{g}$ and R. We provide further details on this in Appendix C, which the reader can skip without losing continuity.

The angular momentum then takes the form:

$$J = \frac{\partial L(\omega)}{\partial \omega} = 2\beta\omega + 4\gamma\omega^3 + \mathcal{O}(\omega^5). \tag{48}$$

While there is no exact method to invert this relation, our assumption of a small ω implies that J must also be small. This allows us to propose an inverse series expansion: $\omega = \omega_1 J + \omega_3 J^3 + \cdots$. By substituting this ansatz back into the previous equation and matching coefficients order by order, we find:

$$\omega = \frac{1}{2\beta} J - \frac{\gamma}{4\beta^4} J^3 + \mathcal{O}(J^5). \tag{49}$$

Finally, we perform the Legendre transformation to obtain the Hamiltonian:

$$H(J) = \alpha + \frac{1}{4\beta} J^2 - \frac{\gamma}{16\beta^4} J^4 + \mathcal{O}(J^6). \tag{50}$$

We can carry out this procedure systematically to compute the Hamiltonian to arbitrarily high orders, provided we can expand the Lagrangian to the corresponding order. We have made an implementation of this method in Wolfram Mathematica available at [14]. We must emphasize that (50) is an approximate result written as a series, and its convergence requires careful study. We refer the reader to Appendix B for a deeper discussion on this point, though it may be skipped without loss of continuity. In addition, looking at (50) up to order $\mathcal{O}(J^2)$, it becomes clear that β represents (up to a factor of 2) the leading order contribution to the moment of inertia of the soliton.

With the Hamiltonian for classical Brane-Skyrmions formulated as a power series in J^2, the quantization process is straightforward. We simply promote J^2 to a quantum mechanical operator, $\hat{J}^2$, which has well-established eigenvalues and eigenstates:

$$\hat{J}^2 \left|j\right\rangle = j(j+1) \left|j\right\rangle, \ \left|j\right\rangle \in \mathcal{H}. \tag{51}$$

Here, $\mathcal{H}$ is the Hilbert space spanned by the eigenstates of the operator $\hat{J}^2$. These states are labeled by the quantum number j, representing the total angular momentum of the soliton.

Notice that the states $|j\rangle$ are simultaneously eigenstates of any power of $\hat{J}^2$:

$$(\hat{J}^2)^n \left|j\right\rangle = j(j+1)(\hat{J}^2)^{n-1} \left|j\right\rangle = \cdots = [j(j+1)]^n \left|j\right\rangle. \tag{52}$$

With this in mind, we promote the classical Hamiltonian to a corresponding quantum operator acting on $\mathcal{H}$:

$$\hat{H} = \sum_{n=0}^{\infty} H_{2n} (\hat{J}^2)^n, \tag{53}$$

where the factors H_{2n} denote the coefficients of the classical series expansion (50). Further details can be found in Appendix C.

We then evaluate the energy of the soliton as the eigenvalue of this quantum mechanical Hamiltonian:

$$\hat{H} \left|j\right\rangle = E_j \left|j\right\rangle = \sum_{n=0}^{\infty} H_{2n} (\hat{J}^2)^n \left|j\right\rangle = \sum_{n=0}^{\infty} H_{2n} [j(j+1)]^n \left|j\right\rangle. \tag{54}$$

This gives the final expression for the quantum mechanical energy eigenvalue:

$$E_j[F] = \sum_{n=0}^{\infty} H_{2n}[F][j(j+1)]^n. \tag{55}$$

We must keep in mind that the energy of the soliton remains a functional of its profile $F(r)$. Additionally, the model contains two free parameters that characterize the profile $F(r)$: the total angular momentum j and the effective coupling λ. The value of j dictates the specific particle state we want to describe. For example, we use $j = 1/2$ for a nucleon and $j > 1/2$ for higher resonances. Thus, for each chosen value of j, we obtain a distinct energy functional that we must minimize with respect to $F(r)$ for a given λ.

Finally, we should briefly address the convergence of the energy series (55). Mathematically, the Lagrangian series $L(\omega)$ converges rapidly in the slow-rotation regime. For this reason, the classical Hamiltonian $H(J)$ also converges for sufficiently small J. However, canonical quantization replaces the continuous classical variable J^2 with discrete quantum eigenvalues $j(j+1)$. As a result, this perturbative expansion remains physically rigorous only for low-lying spin states. Highly excited states with large j would dynamically deform the soliton, breaking the initial assumption of a spherically symmetric ansatz. We will discuss again this issue when analyzing our numerical results.

Numerical results and Experimental fit. To extract numerical results, we must minimize the energy functional (55) for specific values of λ and j. Both parameters, however, scale with the undetermined combination fR_B. We therefore introduce the following rescaled dimensionless parameters:

$$\lambda^* = \frac{\lambda}{f^2 R_B^2}, \quad J^* = \frac{J}{f^4 R_B^4}, \tag{56}$$

where $J \equiv \sqrt{j(j+1)}$. The scaling powers $(fR_B)^n$ emerge naturally when working with the dimensionless energy: $E^* = E/f^4R_B^3$. As a result, J^* acts as an unconstrained parameter for the PINN, rather than representing the physical spin of the nucleon. To relate our numerical results to physical observables, we must fix our free parameters $\{f, R_B, J^*, \lambda\}$ by fitting them to experimental data.

Following [9], we use the nucleon mass M_N and the nucleon isoscalar root mean square (RMS) radius r_N, fixing the spin to $J_N = \sqrt{3/4}$ ($j_N = 1/2$). This allows us to determine three out of the four parameters: f, R_B, and J^*. We fix λ^* prior to the fit because leaving it as an undetermined variable would make the numerical problem significantly more complex.

We identify the theoretical mass with the energy (55) of the soliton configuration. On the other hand, the theoretical isoscalar radius, is defined through the baryonic density $\rho_B(r)$:

$$\langle r^2 \rangle_{I=0} = \int_0^\infty \mathrm{d}r\, r^2 \rho_B(r). \tag{57}$$

We can uniquely determine the baryonic density by requiring its volume integral to yield the total baryon number, which is 1 in our case:

$$B = \int_0^\infty \mathrm{d}r\, \rho_B(r) = 1. \tag{58}$$

Recall that the topological winding number of the Brane-Skyrmion under consideration is also $n_W = 1$. Indeed, we identify these two quantities by setting $B \equiv n_W$, identically to the standard Skyrme model [9]. Since the mapping topology exclusively determines the topological winding number (see, e.g., [16], Sec. 3.2), we can write the baryon number as:

$$B = -\frac{1}{2\pi^2} \int_{\mathbb{R}^3} \mathrm{d}V^* = -\frac{2}{\pi} \int_0^\infty \mathrm{d}r\, F'(r) \sin^2 F(r), \tag{59}$$

where $\mathrm{d}V^*$ denotes the pullback of the volume form $\mathrm{d}V$ from the target 3-sphere[4]. We conventionally introduce the minus sign to ensure $B = 1$ under the boundary conditions $F(\infty) = 0$ and $F(0) = \pi$.

From this, we identify the radial baryonic density as:

$$\rho_B(r) = -\frac{2}{\pi} F'(r) \sin^2 F(r). \tag{60}$$

Notice that this baryonic density exactly matches the one derived in the original Skyrme model [9], as it stems purely from the topological winding of the hedgehog mapping rather than the specific dynamical metric of the brane.

To match the dimensionless PINN outputs with empirical data, we define the dimensionless energy $E^* = E/f^4R_B^3$ and radius $r^* = \frac{1}{R_B}\sqrt{\langle r^2 \rangle_{I=0}}$. We impose the system of equations $M_N = E(J_N, \lambda)$ and $r_N^2 = \langle r^2 \rangle_{I=0}(J_N, \lambda)$, alongside the scaling relation $J_N = f^4 R_B^4 J_N^*$. In principle, these four equations are enough to fix the three free parameters (f, R_B, and J^*) for a given λ^*. However, this system is highly non-linear with respect to J^*, making direct evaluation computationally prohibitive. We adopt a more robust algebraic strategy by defining the following ratio:

$$\frac{M_N r_N}{J_N} = \frac{E^*(J_N^*, \lambda^*) r^*(J_N^*, \lambda^*)}{J_N^*}. \tag{61}$$

This isolates the dependencies into a two-step procedure. First, the PINN computes the outputs across a scan of

[4] "Pullback" means evaluating the volume form of the target manifold S^3 using the coordinates of our base space $\mathbb{R}^3$, as induced by the hedgehog mapping of the branon fields. Essentially, it acts as a geometric coordinate transformation.

λ^* (input)	J_N^*	R_B (fm)	f (MeV)	λ	M_Δ (MeV)
0.01	0.049	77.5	5.2	0.04	938.0
0.10	0.918	5.6	34.9	0.10	949.4
0.50	1.920	5.7	28.2	0.33	998.5
0.80	5.720	1.8	67.1	0.31	1155.1
1.00	7.390	1.5	75.9	0.34	1032.1

TABLE I. Results of the phenomenological fit for the free parameters f, R_B and J^* given a previously fixed value of λ^*. The mass of the Delta resonance stands as a prediction.

J_N^*. The optimal configuration is the one that matches the empirical ratio for each λ^*:

$$\frac{M_N r_N}{J_N} \approx 3.957, \tag{62}$$

using the values $M_N \approx 939\,\text{MeV}$ and $r_N \approx 0.72\,\text{fm}$ ($\hbar c \approx 197.3\,\text{MeV fm}$) [17]. After fixing J_N^* for a given λ^*, we obtain the physical parameters via algebraic substitution:

$$R_B = \frac{r_N}{r^*}, \quad f = \frac{1}{R_B}\left(\frac{J_N}{J_N^*}\right)^{1/4}, \quad \lambda = f^2 R_B^2 \lambda^*. \tag{63}$$

Following this methodology, we can fix the free parameters $\{f, R_B, J^*\}$ for different values of λ^* and obtain predictions such as the mass M_Δ of the Delta resonance ($j_\Delta = 3/2$, $J_\Delta = \sqrt{15/4}$). Table I summarizes these results.

These results show that the limit $\lambda \to 0$ is a poor approximation for describing hadronic spectra, as the prediction for M_Δ is far from the experimental value ($M_\Delta \approx 1232\,\text{MeV}$ [17]). In fact, we obtain $M_\Delta \approx M_N$ in this limit. This happens because the rotational kinetic energy scales inversely with the moment of inertia ($\propto J^2/\mathcal{I}$). The stable configuration found by the PINN yields a massive moment of inertia that dampens the mass splitting.

In contrast, have found that the fit that best predicts the mass of the Delta resonance corresponds to $\lambda^* \approx 0.8$. However, we obtain $J_N^* = 5.72$ for $\lambda^* = 0.8$, giving $J_\Delta^* = \sqrt{5} J_N^* = 12.8$. These values are much larger than unity, meaning the convergence of the series (55) is no longer guaranteed. Our results suggest that the Delta resonance cannot be accurately described with a simple rigid rotation ansatz.

Lastly, let us look at the profiles for different values of λ and j ($J = \sqrt{j(j+1)}$) in physical units. Since $F(r)$ is dimensionless, we only need to rescale the radial coordinate: $r = R_B r^*$. The results are shown in Figure 3.

We see that for small λ, the profiles for different values of j are almost identical, reflecting the heavily constrained mass splitting. When λ is sufficiently large, we can clearly distinguish the profiles, as seen for $\lambda = 0.34$ ($\lambda^* = 1$). It is particularly noteworthy that as $\lambda \to 0$, the energy tends to concentrate near the origin. The energy density scales as $F'(r)$ (16), meaning there is more energy where $F(r)$ is steeper (see the red curve in Figure 3). Essentially, the dynamic solution tends to be highly localized near $r = 0$ as $\lambda \to 0$, while solutions tend to disperse more for larger λ. In Section II, we saw that a static Brane-Skyrmion is point-like for $\lambda \to 0$. Now we have shown that for $\lambda \to 0$, the dynamic solution is highly localized but not point-like, contrary to the static case.

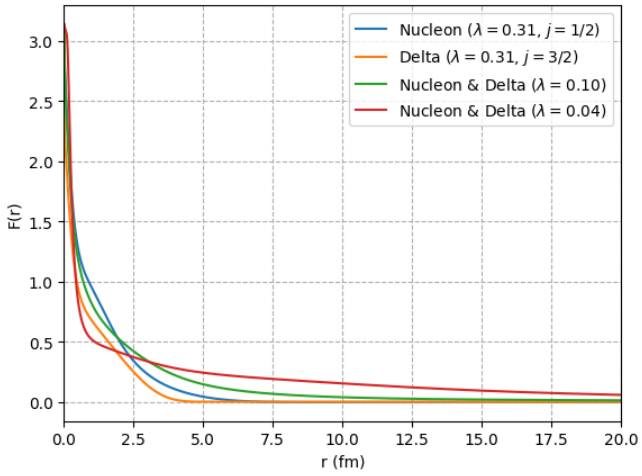

FIG. 3. Brane-Skyrmion profiles of a Nucleon and Delta resonance for different values of λ in physical units. The profiles for small λ are mostly identical for different values of j.

We can understand this evasion of collapse through a scaling argument similar to Derrick's theorem [10]. Applying the scaling $r = L\tilde{r}$ to the Hamiltonian (54) and taking $L \to 0$ (in the $\lambda = 0$ case), we obtain (C6):

$$L_{2n}(L) = \frac{4\pi}{4n^2-1}\int_0^\infty \mathrm{d}\tilde{r}\, L f^4 \sqrt{1 + \frac{R_B^2}{L^2}F'^2(\tilde{r})} \times \left(\frac{v^2}{f^4}\frac{L^2\tilde{r}^2\sin^2 F(\tilde{r})}{L^2\tilde{r}^2 + R_B^2\sin^2 F(\tilde{r})}\right)^n. \tag{64}$$

For $n = 0$, we recover the static $L \to 0$ limit: $H_0 = 2\pi^2 f^4 R_B^3$. However, for $n \geq 1$, Derrick's scaling requires $L_{2n} \to 0$. Crucially, since $L_2 = \beta \to 0$ represents the moment of inertia, the rotational kinetic energy ($\propto J^2/\beta$) diverges. This angular momentum creates a powerful centrifugal barrier that strictly prevents collapse, dynamically forcing the Brane-Skyrmion to adopt a finite size and an energy greater than $2\pi^2 f^4 R_B^3$.

This same argument explains the mass splitting for small values of λ. While J defines the specific quantum states, the induced curvature ($\lambda \neq 0$) provides the dominant energy contribution. Although regimes with $J^* \gtrsim 1$ are possible, we must rigorously verify that successive terms in the series expansion decrease monotonically. As we have seen, this condition is not universally guaranteed for arbitrary configurations.

IV. CONCLUSIONS

This work establishes the canonical quantization of Brane-Skyrmions. We first demonstrated that the standard Atiyah-Manton ansatz is not universally valid for these topological defects, even in purely static configurations, in clear contrast to the standard Skyrme model. By promoting the global symmetries to time-dependent collective coordinates, we successfully quantized the Brane-Skyrmions as a rigid rotor, fulfilling the primary objective of this thesis. Furthermore, to overcome the highly nonlinear differential equations governing the soliton profile, we implemented Physics-Informed Neural Networks (PINNs) to autonomously minimize the complex energy functionals, bypassing the explicit computation of the equations of motion. We supported our numerical findings through Derrick's scaling theorem, which physically explains how the induced centrifugal barrier prevents the collapse of the quantum solitons and accounts for the point-like nature of classical defects.

In the last section, we performed a phenomenological fit to model physical nucleons, similar to the original Skyrme approach. We found that states with spin $j > 1/2$ are not well described by a rigid rotation ansatz. The series expansion becomes non-convergent for these highly spinning states, and the PINN yields a massive moment of inertia in the limit $\lambda \to 0$ that severely dampens the mass splitting $M_\Delta - M_N \sim J^2/\mathcal{I}$. In addition, by forcing the Δ resonance ($j = 3/2$) to adopt the exact same static profile as the nucleon ($j = 1/2$), we ignore the "centrifugal stretching" effect. In a fully dynamic, nonperturbative quantization, the stronger centrifugal barrier of the Δ state would physically deform and expand the soliton, altering its inertial properties and potentially correcting the mass spectrum. Developing a fully nonperturbative approach to capture this dynamic deformation remains an open computational challenge, althugh it may be the key to a mo re accurate description of the hadronic mass spectrum.

Despite these phenomenological limitations, our Brane-Skyrmion model presents a significant theoretical advantage over the standard Skyrme model. The standard Skyrme approach captures just the lowest-order contribution in J^2 for the rotational kinetic energy. The Dirac-Nambu-Goto nature of our effective action provides a systematic expansion to arbitrary higher orders in J^2. These higher-order terms could introduce highly valuable corrections to the physics of spinning hadronic resonances. While the standard Skyrme equations can be solved using traditional shooting methods, the analytical complexity of Brane-Skyrmions makes such approaches prohibitive. The successful implementation of PINNs in this work bypassed these analytical obstacles and highlighted the immense potential of neural networks as unsupervised solvers in modern theoretical physics.

While there is room for improvement, this work establishes a robust framework for exploring topological solitons within extra-dimensional theories. Having successfully formulated the semiclassical quantization, the model opens numerous avenues for future research. On the fundamental scale, the higher-order spin corrections derived here could deepen our understanding of chiral dynamics and the spectrum of excited baryons. On the macroscopic scale, applying this quantized framework to astrophysical environments presents an extraordinary frontier. Generalizing Brane-Skyrmions to multi-soliton configurations could yield a novel Equation of State (EoS) for the dense nuclear matter inside neutron stars, just as researchers do today within the standard Skyrme framework [18]. Comparing such an EoS with the latest astrophysical observables, such as maximum pulsar masses and gravitational wave signatures, could provide a profound link between the geometry of extra dimensions and the observable universe.

REFERENCES

[1] T. Kaluza, International Journal of Modern Physics D **27**, 1870001 (2018).
[2] O. Klein, Z. Phys. **37**, 895 (1926).
[3] N. Arkani-Hamed, S. Dimopoulos, and G. R. Dvali, Phys. Lett. B **429**, 263 (1998), arXiv:hep-ph/9803315.
[4] V. A. Rubakov and M. E. Shaposhnikov, Phys. Lett. B **125**, 136 (1983).
[5] A. Dobado and A. L. Maroto, Nucl. Phys. B **592**, 203 (2001), arXiv:hep-ph/0007100.
[6] T. H. R. Skyrme, Proc. Roy. Soc. Lond. A **260**, 127 (1961).
[7] J. K. Perring and T. H. R. Skyrme, Nucl. Phys. **31**, 550 (1962).
[8] J. A. R. Cembranos, A. Dobado, and A. L. Maroto, Phys. Rev. D **65**, 026005 (2002), arXiv:hep-ph/0106322.
[9] G. S. Adkins, C. R. Nappi, and E. Witten, Nucl. Phys. B **228**, 552 (1983).
[10] G. H. Derrick, J. Math. Phys. **5**, 1252 (1964).
[11] A. Garoffolo, K. Hinterbichler, and M. Trodden, JHEP **09**, 115, arXiv:2505.08865 [hep-th].
[12] M. F. Atiyah and N. S. Manton, Phys. Lett. B **222**, 438 (1989).
[13] H. Wang, L. Lu, S. Song, and G. Huang, Communications in Computational Physics **34**, 869–906 (2023).
[14] S. Sánchez, Topological-solitons-PINNs (2026), GitHub repository. Accessed: June 7, 2026.
[15] R. Luna, Machine learning for strong gravity, accessed: 2026-07-01.
[16] N. S. Manton and P. Sutcliffe, *Topological solitons*, Cambridge Monographs on Mathematical Physics (Cambridge University Press, 2004).
[17] S. Navas *et al.* (Particle Data Group), Phys. Rev. D **110**, 030001 (2024).
[18] A. García Martín-Caro, *Solitons and effective field theories in the Physics of strong interactions*, Ph.D. thesis, Santiago de Compostela U. (2023).

Appendix A: Shooting Method

The shooting method is a numerical technique designed to solve second-order boundary value problems. It is particularly useful when we know two boundary conditions for a function $F(r)$, but we lack an initial condition for its derivative $F'(r)$.

For the specific case of static Brane-Skyrmions, we need to solve the nonlinear differential equation obtained by extremizing the radial energy functional:

$$M_S[F] = -4\pi \int_0^\infty \mathrm{d}r\, \mathcal{L}_{\text{eff}}[F, F', F''; r], \tag{A1}$$

where $\mathcal{L}_{\text{eff}} = (f^4 - \lambda f^2 R)\sqrt{g}$. We can safely omit the vacuum energy term $M_S[0]$, since it acts as a constant shift and is therefore completely irrelevant to the resulting equations of motion.

At first glance, one might expect the corresponding Euler-Lagrange equations to be of fourth order because the scalar curvature R introduces second derivatives (F'') into the Lagrangian. However, the term $R\sqrt{g}$ corresponds exactly to the Einstein-Hilbert action for the induced metric. It is a well-known result that the second derivatives within this term can be integrated by parts, leaving only a boundary contribution. As a result, the variational principle yields a strictly second-order, nonlinear ordinary differential equation (ODE) for the profile $F(r)$. We confirmed this conclusion by deriving the equation symbolically using Wolfram Mathematica.

To solve this ODE numerically, we use the shooting method and define the first derivative at the origin as the shooting parameter s, setting $F'(0) = -s$. Knowing the boundary condition $F(0) = \pi$, we approximate the solution near the origin as $F(r) \approx \pi - sr$ for sufficiently small $r > 0$. We avoid $r = 0$ strictly to prevent numerical singularities. This step initializes the integration. We then integrate the ODE outward, which gives a parametric solution dependent on s. We then iteratively adjust the parameter s until the asymptotic boundary condition is satisfied, meaning $F(\infty) = 0$.

We implemented this numerical procedure in the Wolfram Mathematica notebook available at [14]. We used it as an independent benchmark to validate the accuracy of the PINN approach. This allows for a direct comparison of both solutions, as shown in Figures 1 and 2.

We observe that the solutions provided by the shooting method and the PINN mostly coincide. This justifies the use of PINNs over traditional numerical methods. The neural network is significantly more versatile because it does not require explicit knowledge of the equations of motion. In fact, the network performs the minimization autonomously via automatic differentiation directly on the energy functional (as detailed in Appendix B). This capability becomes a vital advantage during quantization, where the effective Hamiltonian lacks a straightforward density representation.

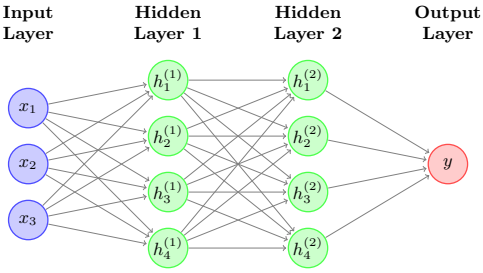

FIG. 4. Generic multi-layer neural network diagram.

Appendix B: Neural network (NN)

We begin by outlining the architecture of a generic neural network, as shown in Figure 4. The general structure consists of an **input layer**. This layer acts as a column vector representing the features of a single dataset, such as spatial coordinates, and contains the initial variables to be processed.

The network then processes this dataset through a set of **hidden layers**. Each layer applies a linear transformation to the output of the previous one, followed by a non-linear activation function. Mathematically, the output of a given layer is $\mathbf{h} = \sigma(\mathbf{W}\mathbf{x} + \mathbf{b})$, where $\mathbf{W}$ is the weight matrix, $\mathbf{b}$ is the bias vector, and σ is the activation function. This non-linearity gives the network the ability to model highly complex phenomena. The **output layer** yields the final prediction of the model once all transformations through the hidden layers are complete.

With the architecture established, we can describe the standard learning process:

1. **Forward pass:** The model receives the input data and generates its prediction as described above.

2. **Loss function:** In supervised learning, a *loss function* compares the prediction against a known expected value to quantify the error.

3. **Backpropagation:** The algorithm uses the chain rule to compute the gradient of the loss function with respect to each network parameter.

4. **Optimization:** An optimization algorithm updates the weights and biases based on the computed gradients to reduce the error in the next iteration. This cycle repeats until the loss function reaches an acceptable minimum or meets a predefined tolerance criterion.

Training a neural network is essentially an optimization problem. In the specific context of PINNs, the input is a set of spatial coordinates $\mathbf{x}$ and the output is a continuous function $f(\mathbf{x})$. Instead of relying on labeled data, we replace the traditional loss function with a physical functional $\mathcal{F}[f]$, such as the total energy of the system. The network learns to find the physical configuration that minimizes this energy directly, avoiding the need for prior experimental data.

Appendix C: Hamiltonian coefficients

We recall that the classical Hamiltonian for spherical Brane-Skyrmions can be expressed as a power series in J^2:

$$H(J) = \sum_{n=0}^{\infty} H_{2n} J^{2n} = \alpha + \frac{1}{4\beta} J^2 - \frac{\gamma}{16\beta^4} J^4 + \mathcal{O}(J^6), \tag{C1}$$

provided that $H_{2n} J^{2n} \gg H_{2(n+1)} J^{2(n+1)}$. This condition ensures the convergence of the series in the slow-rotation regime.

The parameters α, β, γ, and higher-order terms correspond to the coefficients of the classical Lagrangian expansion:

$$L(\omega) = \sum_{n=0}^{\infty} L_{2n} \omega^{2n} = -\alpha + \beta\omega^2 + \gamma\omega^4 + \mathcal{O}(\omega^6). \tag{C2}$$

We derive these coefficients by substituting the expansions of (41) and R:

$$\sqrt{g} = \sqrt{g_0} \sum_{n=0}^{\infty} A_n C^n(r) \sin^{2n}\theta \omega^{2n}, \quad R = \sum_{n=0}^{\infty} R_{2n} \omega^{2n}, \tag{C3}$$

where

$$A_0 = 1, \quad A_n = -\frac{(2n-2)!}{2^{2n-1} n! (n-1)!}, \quad n \geq 1. \tag{C4}$$

The terms R_{2n} denote the coefficients of the scalar curvature expanded in powers of ω^2. We compute these symbolically using Wolfram Mathematica [14].

We note that A_0 is strictly positive, while A_n is negative for $n \geq 1$. This change in sign explains why we define $L_0 = -\alpha$ and $L_{2n} = \{\beta, \gamma, \dots\}$ for $n \geq 1$. Combining these expansions with the total Lagrangian (45) and grouping terms order by order gives the following general expression:

$$L_{2n} = \int \mathrm{d}^3x \sqrt{g_0} \Big[A_n(-f^4 + \lambda f^2 R_0) C^n(r) \sin^{2n}\theta + \lambda f^2 \sum_{k=0}^{n-1} A_k R_{2n-2k} C^k(r) \sin^{2k}\theta \Big], \tag{C5}$$

where the coordinates span $r \in [0, \infty)$, $\theta \in [0, \pi)$, and $\phi \in [0, 2\pi)$. The term $\sqrt{g_0}$ is given by (10) and $C(r)$ by (42).

Evaluating these coefficients in the $\lambda = 0$ limit is very useful, as they take the following closed-form expression:

$$L_{2n} = \frac{4\pi}{4n^2 - 1} \int_0^{\infty} \mathrm{d}r \, f^4 \frac{\sqrt{g_0}}{\sin\theta} C^n(r), \tag{C6}$$

where the quotient $\sqrt{g_0}/\sin\theta$ is independent of θ and solely a function of r.

The first three coefficients are:

$$\alpha(\lambda = 0) = 4\pi \int_0^{\infty} \mathrm{d}r \, f^4 \frac{\sqrt{g_0}}{\sin\theta}, \tag{C7}$$

$$\beta(\lambda = 0) = \frac{4\pi}{3} \int_0^{\infty} \mathrm{d}r \, f^4 \frac{\sqrt{g_0}}{\sin\theta} C(r), \tag{C8}$$

$$\gamma(\lambda = 0) = \frac{4\pi}{15} \int_0^{\infty} \mathrm{d}r \, f^4 \frac{\sqrt{g_0}}{\sin\theta} C^2(r). \tag{C9}$$

To properly analyze the convergence of the effective Lagrangian series, we must examine the dimensionless expansion parameter $\omega^2 C(r)$. By definition (42), $C(r)$ has dimensions of length squared. Because we assume $\omega \ll 1$, and $C(r)$ is bounded over the entire radial domain ($C(r) \to 0$ as $r \to 0$ and $r \to \infty$), the condition $\omega^2 C(r) \ll 1$ holds uniformly. As a result, consecutive terms in the Lagrangian density scale as $(\omega^2 C)^{n+1} \ll (\omega^2 C)^n$. This directly leads to $L_{2(n+1)} \omega^{2(n+1)} \ll L_{2n} \omega^{2n}$. This confirms that the power series expansion converges safely for $\lambda \to 0$. It fully justifies truncating the series at the first few orders in J^2.